Journal of Statistical Physics, Vol. 76, Nos. 5/6, 1994

Pruning-Induced Phase Transition Observed by a Scattering Method

Wolfgang Breymann[1] **and Jürgen Vollmer**[1]

Received January 26, 1994

In hyperbolic systems, transient chaos is associated with an underlying chaotic saddle in phase space. The structure of the chaotic saddle of a class of piecewise linear, area-preserving, two-dimensional maps with overall constant Lyapunov exponents has been observed by a scattering method. The free energy obtained in this way displays a "phase transition" at $\beta < 0$ in spite of the fact that no phase transition occurs in the free energy dedcued from the spectrum of Lyapunov exponents. This is possible because pruning introduces a second effective scaling exponent by creating, at each level of the approximation, particular small pieces in the incomplete Cantor set approximating the saddle. The second scaling arises for a subset of values of the control parameter that is dense in the parameter interval.

KEY WORDS: Thermodynamic formalism; phase transition; chaotic scattering; piecewise linear maps; bifurcation.

1. INTRODUCTION

Invariant sets of chaotic dynamical systems are generally multifractals. They can be characterized by their multifractal properties (probabilities), their hierarchy of length scaling exponents (geometrical properties), and their spectrum of Lyapunov exponents (dynamical properties). In the case of hyperbolic systems, these quantities are related to each other by relations following from the thermodynamic formalism.[1]

Chaotic invariant sets are created by homoclinic or heteroclinic intersections of stable and unstable manifolds. If all branches of the stable bundle intersect all branches of the unstable bundle, the invariant set is topologically equivalent to a complete two-dimensional (2D) Cantor set. Under variation of an external control parameter, the grid of intersections

[1] Institut für Physik, Universität Basel, CH-4056 Basel, Switzerland.

0022-4715/94/0900-1439$07.00/0

frequently become incomplete. Consequently, parts of the invariant set get lost. This phenomenon is called "pruning."

Due to time reversal symmetry in Hamiltonian systems, the bundles of stable and unstable manifolds are equivalent, and their partial fractal properties are the same.[2] In order to know the structure of the invariant set, it is sufficient to study the structure of the stable manifolds, i.e., to investigate orbits only for $t \to \infty$. The properties of the invariant set are reflected in the behavior of transient orbits. A possible appearance of transient chaos in Hamiltonian systems is chaotic scattering. Numerical "scattering experiments" are an efficient tool for investigating the structure of the invariant manifolds in such systems.[3] They can be performed by choosing a line $I^{(0)}$ of initial conditions outside the invariant set in such a way that the line crosses all branches of the stable manifolds of this set. The invariant set, which is in fact a hyperbolic saddle, acts as the scattering region. The trajectories starting out of $I^{(0)}$ will enter the invariant set and eventually leave it after some delay. The closer an initial point is located to a branch of the stable manifolds, the longer is the time delay, which becomes infinite for initial points located on a manifold. Thus, the stable manifolds give rise to a Cantor set of hierarchically organized singularities in the time delay function. The union of (closed) subintervals of $I^{(0)}$ for which the time delay is greater than or equal to some finite value n provides an n-level approximation of this set. The statistics of scaling exponents in the set is equivalent to the statistics of scaling exponents in the full invariant set of the dynamical system.

In the framework of the thermodynamic formalism, a formal "free energy" provides the statistics of length scaling exponents. This free energy can be derived from the set of singularities of the time delay function as well as from the spectrum of Lyapunov exponents of the periodic orbits. In hyperbolic systems, the spectrum of Lyapunov exponents and the spectrum of length scaling exponents are expected to be equivalent.

We investigated the free energy for a family of piecewise linear, area-preserving maps. Piecewise linear maps are readily used as models since they can be iterated quickly on a computer and they are nearly the only maps that allow analytical calculations. Well-known 2D examples are the baker's transformation (e.g., ref. 5) as a model for Hamiltonian systems and piecewise linear maps studied by Lozi[6] and Tél[7] as models for dissipative systems. For some parameter values, however, the latter are area-preserving. The one-parameter family studied in this paper has been used to describe the metastable states of a chain with anharmonic nearest-neighbor and harmonic next-nearest-neighbor interactions.[8,9] Furthermore, it describes[10] the dynamics of a billiard in a gravitational field.[11] It also occurs as limiting case of a family of smooth maps describing the

stable states of an optical memory.[12] The surprising result of this paper is that for this class of piecewise linear 2D maps, the spectrum of Lyapunov exponents is not equivalent to the spectrum of length scales obtained by the scattering method. In the scattering free energy, an additional scaling exponent and a phase transition (in the sense of the thermodynamic formalism) occur, which are not present in the free energy calculated through the periodic orbits of the invariant set. Technically this is possible because hyperbolicity is violated. "Physically," the occurrence of the anomalous behavior of the scattering free energy is related to pruning of orbits in the invariant set.

In Section 2 the family of piecewise linear maps is introduced and the free energy is derived from the Lyapunov exponents; it shows a regular behavior. Numerical results for the scattering free energy are presented in Section 3. They exhibit an additional scaling exponent and a phase transition for negative β values. The theoretical analysis in Section 4 corroborates these findings. It reveals that the anomalous effects are closely related to pruning and occur for a subset of parameter values that lies dense in the interval of the external control parameter. The paper concludes with a summary and discussion (Section 5).

2. THE MODEL SYSTEM

The one-parameter family of maps f studied in the following is defined on the whole real plane as

$$f: \begin{pmatrix} x_{n+1} \\ y_{n+1} \end{pmatrix} = \begin{cases} \begin{pmatrix} \eta & 0 \\ 0 & \eta^{-1} \end{pmatrix} \begin{pmatrix} x_n \\ y_n \end{pmatrix} & \text{for } l(x_n, y_n) \leqslant 0 \\ \begin{pmatrix} \eta & 0 \\ 0 & \eta^{-1} \end{pmatrix} \begin{pmatrix} x_n \\ y_n \end{pmatrix} + (1-\eta) \begin{pmatrix} 1 \\ -\eta^{-1} \end{pmatrix} & \text{for } l(x_n, y_n) > 0 \end{cases} \tag{2.1}$$

where the line $l(x, y)$, defined as

$$C: \quad l(x, y) = \eta x + y - \frac{1+\eta}{2} \tag{2.2}$$

separates the two branches of f (Fig. 1). After an appropriate linear coordinate transformation, f corresponds to the area-preserving case of the map $v_{n+1} = av_n - \text{sign}(v_n) + bz_n$; $z_{n+1} = v_n$ with parameters $a = (\eta^2 + 1)/\eta$ and $b = -1$[13] (following the notation of ref. 7). Stretching and folding occur as in the baker's transformation. The map is discontinuous on the line C, which we call *critical line* in analogy to the critical point of 1D maps. Note

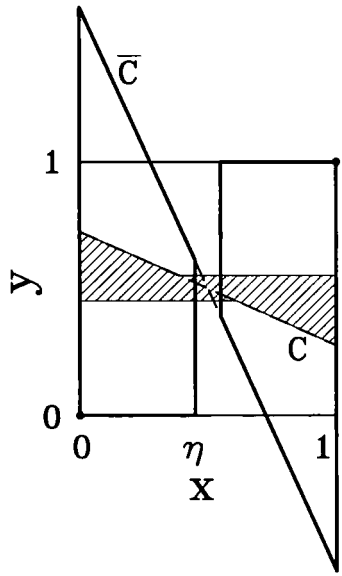

Fig. 1. The generalized baker's transformation for $\eta = 0.45$. The critical line C has slope $-\eta$ and passes through the midpoint P_c of the unit square. Its image $f(C)$ is labeled by $\bar{C}$. The left (right) trapezoid drawn by heavy lines is the image of the part of the unit square mapped by the lower (upper) branch of f. The hatched region is mapped on the parts of the trapezoids outside the unit square. This region is forbidden in the sense that all points which eventually enter it escape to infinity under forward iteration and do not belong to the chaotic saddle.

that such a line of singularities is also present in more general maps of Lorenz-type systems.[14] The piecewise linear map given by Eq. (2.1) is studied for convenience only.

The behavior of f strongly depends on the paramter η. Without loss of generality, the investigation will be restricted to $\eta \in (0, 1)$. For $\eta = 0$, the map is not defined and for $\eta = 1$, it reduces to identity. For the other η values, f has two fixed points, in (0, 0) and (1, 1). Their stable and unstable manifolds (Fig. 2) contain the horizontal and vertical sides of the unit square, respectively. Inside the square, the manifolds give rise to a chaotic invariant set generated by homoclinic and heteroclinic intersections (Fig. 3). Both stable and unstable bundles extend to infinity. The bundle of stable manifolds is composed of horizontal straight line segments confined to a band of width one. For $x \to \infty$, the bundle approaches the $(y = 1)$ line from below and for $x \to -\infty$, it approaches the $(y = 0)$ line from above (Fig. 2a). All points outside the horizontal band escape to $y = \pm\infty$ under iteration of f. The unstable manifolds have the same structure in vertical direction, and points outside the corresponding vertical band escape to $x = \pm\infty$ under f^{-1} (Fig. 2b).

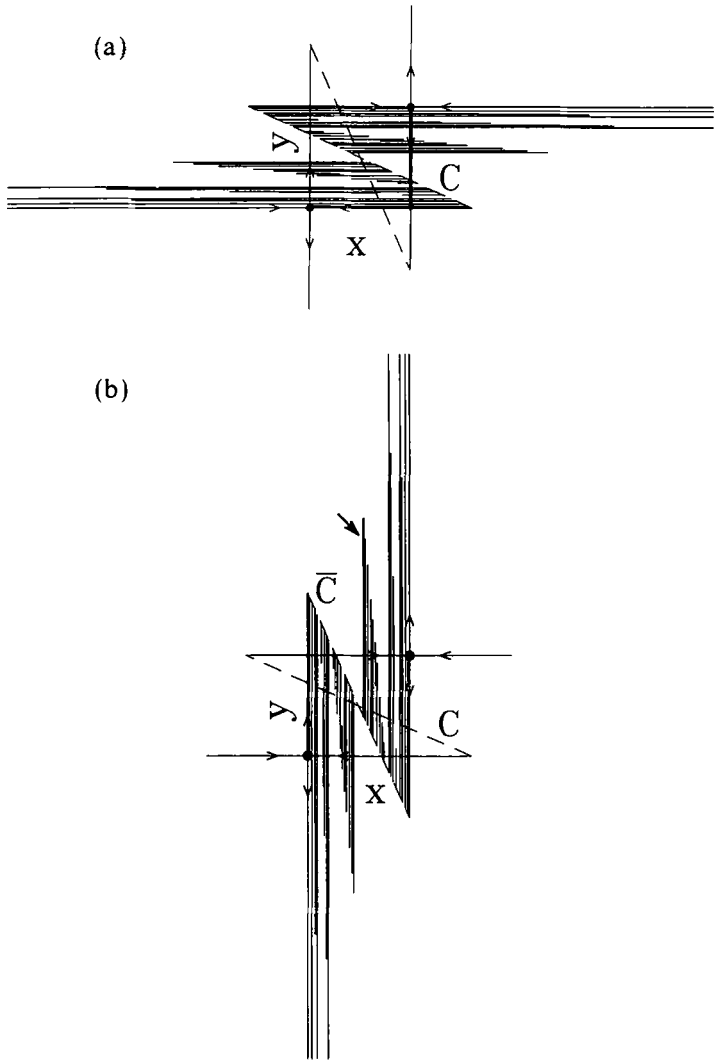

Fig. 2. The stable (a) and unstable (b) manifolds of the fixed points of the generalized baker's transformation shown for the same η value as in Fig. 1. Most of the branches of the stable manifolds start at the critical line C, most of the branches of the unstable manifolds start at its image $\bar{C}$. The heavy line in part (a) is the line of initial conditions $I^{(0)}$ chosen for calculating the time delay function, which yields the input data for the thermodynamic formalism. The unstable manifold of $(0, 0)$ in part (b) starts with the left border of the unit square (heavy line) and extends up to the line $\bar{C}$. The right heavy line (cf. arrow) is the image of the part of the left heavy line between the lines C and $\bar{C}$. It contains the left border of the right trapezoid shown in Fig. 1. For $\eta > 1/3$, this line segment does not completely cross the unit square; its lower endpoint with coordinates $(1-\eta, (3-\eta^{-1})/2)$ lies inside the square.

The upper branch of the unstable manifold of (0, 0) starts with the left border of the unit square and extends up to the first image $\bar{C}=f(C)$ of the critical line (Fig. 2b). The whole branch is obtained by iterating this first piece. For the complete case without pruning ($\eta < 1/3$) all line segments completely cross the unit square, while for $\eta > 1/3$, for which pruning occurs, some segments as the one indicated by the arrow in Fig. 2b start or end inside the square.

The trajectories

$$\{p_k\}_{k=-\infty}^{\infty} = \{\cdots f^{-2}(p_0), f^{-1}(p_0), p_0, f(p_0), f^{(2)}(p_0)\cdots\}$$

of the chaotic invariant set can be labeled by infinite symbol sequences $\cdots\sigma_{-2}\sigma_{-1}\sigma_0\sigma_1\sigma_2\cdots$ composed of binary symbols. The symbol σ_k takes the value 0 or 1 depending on whether p_k lies below or above the critical line. The coordinates of p_k can easily be recovered from the symbol sequence of the orbit.[8, 13] In general, not all symbol sequences correspond to trajectories. The necessary and sufficient condition for a given sequence to be allowed can be written in the form of a self-consistency condition $\sigma_n = h_n(\{\sigma_i\})$ that must be satisfied for all n.[8] Graphically, this condition means that the orbit associated with a point of the invariant set does not enter the forbidden region indicated in Figs. 1 and 3. The self-consistency condition is fulfilled for all points of a regular 2D Cantor set with scaling η as long as the critical line does not intersect the first-level approximation of the Cantor set (Fig. 3a). In this case, the chaotic saddle coincides with the embedding Cantor set. For $\eta > 1/3$, the forbidden regions intersect the Cantor set: Pruning occurs changing the regular structure of the chaotic saddle to an irregular one (Fig. 3b–3d).

The length scaling properties of a dynamically generated fractal are related to the Lyapunov exponents[1] by means of the partition sum

$$Z_{\text{Lyap}}^{(n)}(\beta) = \sum_{\substack{x_0 \text{ point of} \\ \text{period } n}} \exp[-n\beta\lambda_+(x_0)] \propto \exp[-n\beta F_{\text{Lyap}}(\beta)] \qquad (2.3)$$

The proportionality holds in the limit $n \to \infty$. Since for all orbits the positive Lyapunov exponent $\lambda_+(x_0)$ is equal to $\log \eta^{-1}$, the partition sum immediately reduces to

$$Z_{\text{Lyap}}^{(n)}(\beta) = M(n)\, e^{n\beta \log \eta} \qquad (2.4)$$

where $M(n)$ is the number of period-n orbits. In the limit $n \to \infty$, the increase of $M(n)$ with n is governed by the topological entropy. Consequently,

$$\beta F_{\text{Lyap}}(\beta) = -K_0 - \beta \log \eta \qquad (2.5)$$

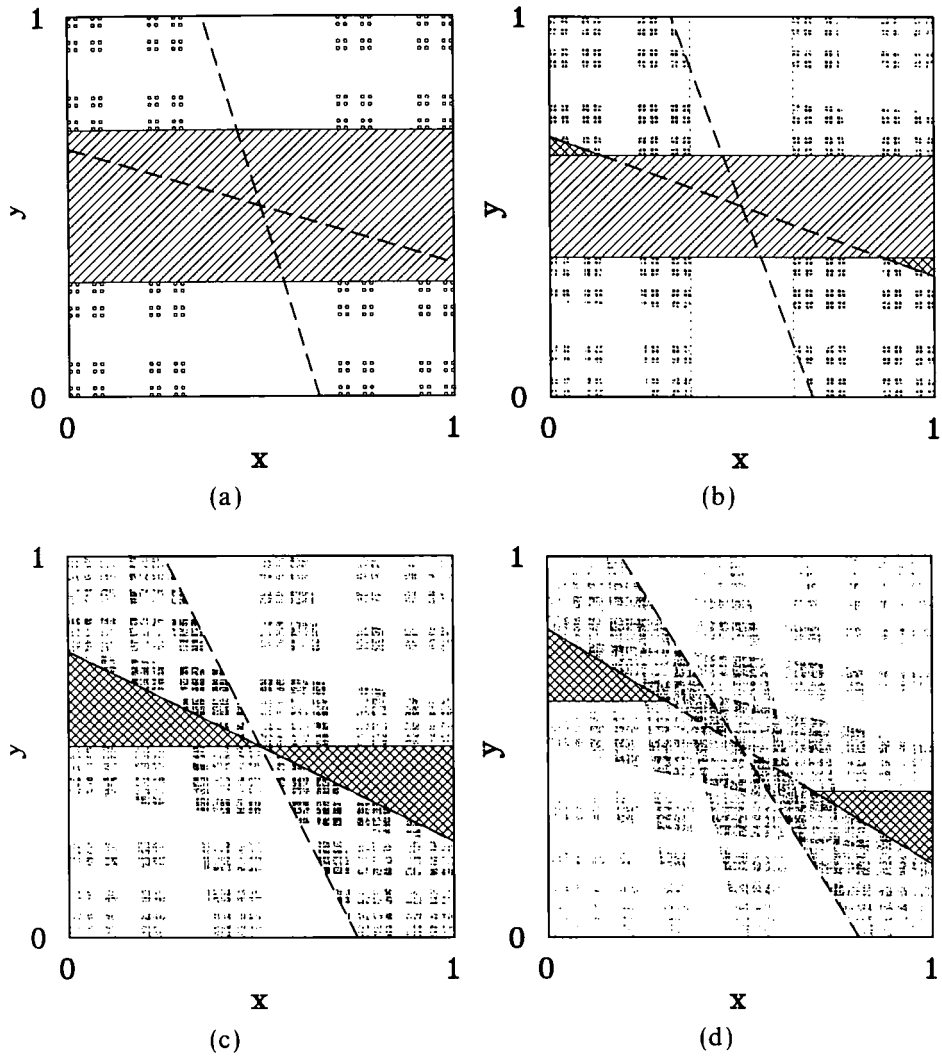

Fig. 3. The chaotic saddle of the map (2.1) for different parameter values. The dashed lines indicate the lines C (slope $-\eta$) and $\bar{C}$ (slope $-\eta^{-1}$). (a) $\eta = 0.3$: The saddle forms a 2D Cantor set created by a complete grid of intersections of stable and unstable manifolds, i.e., all branches of the stable and unstable manifolds completely cross the unit square. The forbidden region forms a horizontal band (hatched area). (b) $\eta = (\sqrt{3}-1)/2 \simeq 0.366$: Pruning manifests itself in the creation of additional triangles (double hatched) at the corners of the forbidden band (hatched). They are due to the intersection of the critical line and the first-level squares of the Cantor set. Note that the structure of the embedding set remains visible. The midpoint of the unit square does not belong to the saddle. (c) $\eta = 1/2$: The forbidden region is composed of two triangels (double hatched), which touch in the center P_c of the unit square. At this parameter value the embedding Cantor set degenerates to the whole unit square; the first-level squares touch in P_c. (d) $\eta = (\sqrt{5}-1)/2 \simeq 0.618 > 0.5$: The two triangles (double hatched) of the forbidden region are well separated.

The graph of $\beta F(\beta)$ vs. β is a straight line. The invariant set is an irregular fractal but not a multifractal; its topological entropy is proportional to its fractal dimension $D_0 = K_0/\log(\eta^{-1})$. The dependence of the topological entropy on η has been investigated in detail in ref. 15.

3. THE FREE ENERGY OBTAINED BY SCATTERING

The time delay function has been calculated for trajectories starting out of a specified line $I^{(0)}$ of initial conditions. For $I^{(0)}$ we chose the right boundary of the unit square, which completely intersects the bundle of stable manifolds (Fig. 2a). Let $I_s^{(n)} \subset I^{(0)}$ label intervals on which the time delay function takes values greater than or equal to n (Fig. 4). By the index s, we consecutively number these level-n intervals, starting with $I_0^{(n)}$ for the lowest-lying one. All orbits $\{p_i\}$ starting out of some interval $I_s^{(n)}$ qualitatively behave in the same way for at least n iterations: Given s and $i = 1,..., n$, the points $p_i = f^{(i)}(p_0)$ with $p_0 \in I_s^{(n)}$ are located either all above or all below the critical line. The symbols $\sigma_i = \sigma_i(s)$ take the same value for

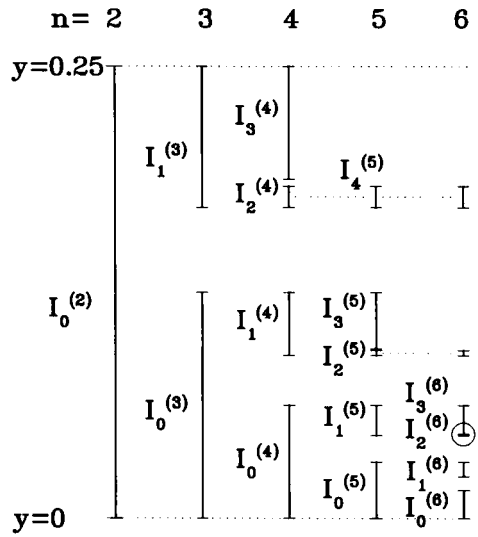

Fig. 4. Hierarchical organization of the intervals $I_s^{(n)} \subset I^{(0)}$, shown for $\eta = 0.5$ and $n = 2,..., 6$. Only the part of $I^{(0)}$ below the intersection of the critical line at $y = 1/4$ is drawn. The successors of $I_3^{(4)}$ and $I_3^{(5)}$ are dropped. At each level n, the intervals $I_s^{(n)}$ are successively numbered, starting with $I_0^{(n)}$ at the lower end of $I^{(0)}$. In the complete case, each level-n interval $I_s^{(n)}$ splits into two level-$(n+1)$ intervals $I_{s'}^{(n+1)}$ and $I_{s'+1}^{(n+1)}$. Since pruning is present, some intervals, such as $I_2^{(4)}$, give rise to only one interval on the next level. Note that for $n \geq 4$, the intervals $I_2^{(n)}$ are the shortest intervals at the nth level (labeled $I_{\min}^{(n)}$ in the text). The series of $I_{\min}^{(n)} = I_2^{(n)}$ scales with $\eta^2 = 2^{-2}$. The lengths of the $I_s^{(n)}$ serve as input data for calculating the partition sum.

all these trajectories. Consequently, the finite subsequence $\sigma_1(s)\cdots\sigma_n(s)$ can be associated to the interval $I_s^{(n)}$. Note that for $k \leqslant n$ the kth image of an interval $I_s^{(n)}$ is a single straight line segment.

Through the lengths $l_s^{(n)}$ of the intervals $I_s^{(n)}$ the scattering process gives access to the partition sum $Z^{(n)}$ and hence to a scattering free energy[3] by

$$Z^{(n)}(\beta) = \sum_s (l_s^{(n)})^\beta \propto e^{-n\beta F(\beta)} \tag{3.1}$$

Again, the proportionality holds asymptotically for large n. We introduce the level-n free energy $F^{(n)}$ as

$$F^{(n)}(\beta) = -\frac{1}{n\beta} \log Z^{(n)}(\beta) \tag{3.2}$$

Because of the asymptotic scaling of $Z^{(n)}(\beta)$ with n, the approximate free energies $\{F^{(n)}(\beta)\}$ tend to $F(\beta)$ in the limit $n \to \infty$. A level-n free energy $F_k^{(n)}(\beta)$ can equally well be defined by comparing the partition sums at level n and $n-k$:

$$\begin{aligned} F_k^{(n)}(\beta) &= -\frac{1}{\beta k} \log \frac{Z^{(n)}(\beta)}{Z^{(n-k)}(\beta)} \\ &= \frac{1}{k} [nF^{(n)}(\beta) - (n-k) F^{(n-k)}(\beta)] \end{aligned} \tag{3.3}$$

For a given k, the series $\{F_k^{(n)}(\beta)\}$ do not necessarily converge; but if they do, they converge to $F(\beta)$. If the series $\{F^{(n)}(\beta)\}$ displays a period k, as in the example treated in Section 4.1.3, the series $\{F_k^{(n)}(\beta)\}$ have the advantage of converging faster than $\{F^{(n)}(\beta)\}$. Indeed, the latter contains a term proportional to a $1/n$ convergence which drops out in the second line of Eq. (3.3) by taking the difference.

Figures 5a and 5b display the level-n free energies $\beta F^{(n)}(\beta)$ and $\beta F_1^{(n)}(\beta)$ for $\eta = 1/2$ and $n = 10$, 15, 20, 25, and 30. They show that the scattering free energy is clearly not a straight line: In both figures, the slope for negative β values is visibly larger than for positive ones. For positive β values the asymptotic behavior, which equals the behavior of F_{Lyap}, is reached in both figures. For negative values of β, however, only Fig. 5b allows a quantitative statement on the asymptotic slope. It supports the hypothesis that for $\beta < \beta_c < 0$, the asymptotic line is given by $\beta F(\beta) = 2\beta \log 2$. This means that the scattering free energy contains an additional scaling exponent $2 \log 2$ not related to the positive Lyapunov exponent of f. The numerical data indicate but do not prove a phase transition at $\beta_c = -K_0/\log 2$. This hypothesis will be corroborated in the next section. A phase transition at a negative β value is the signature for the existence

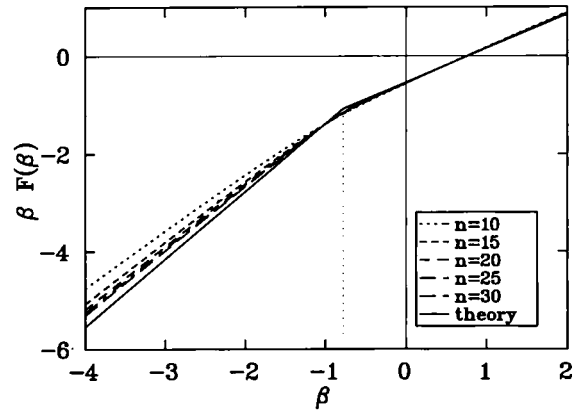

(a)

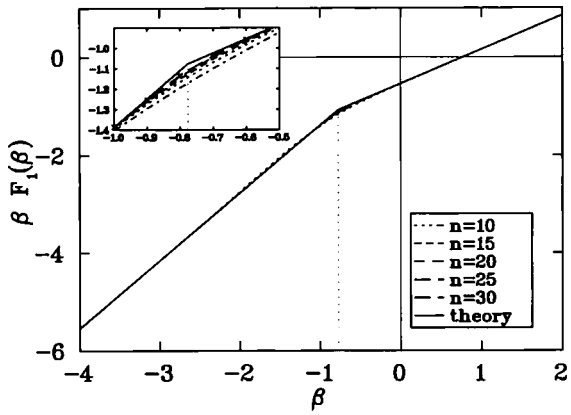

(b)

Fig. 5. Free energy for $\eta = 0.5$ and $n = 10$, 15, 20, 25, and 30 computed numerically by the scattering method. (a) $\beta F^{(n)}(\beta)$. The asymptotic behavior (solid line) is practically reached for positive values of β but not for the negative ones. (b) $\beta F_1^{(n)}(\beta)$. Note the excellent convergence also for negative values of β. The dotted vertical line (in both parts) indicates the critical value β_c at which the phase transition occurs.

of a larger scaling exponent for a "small" number of intervals. Since in the piecewise linear map f the Lyapunov exponents are constant, the additional scaling exponent(s) and the related phase transition can only be caused by pruning.

The question arises whether the anomalous behavior of the scattering free energy is an exceptional phenomenon due to some special properties at $\eta = 1/2$ or whether it is generic for (this and perhaps other families of)

piecewise linear maps with pruning. To get some idea, $\beta F(\beta)$ has been calculated for slightly different η values. The result is very disappointing: $\beta F_1^{(n)}$ gives totally unreliable results for negative β. Even if the slopes of the $\beta F^{(n)}$ are larger for negative β than for positive ones, it is impossible to make any statement on the asymptotic behavior. We show in the next section that the anomaly found in the $\eta = 1/2$ case exists for all parameter values at which a homoclinic or heteroclinic orbit of the invariant set becomes forbidden.

4. PRUNING-INDUCED SECOND SCALING FACTOR

4.1. Three Examples

The results exposed in the previous section indicate that there is a second scaling factor different from η in the chaotic invariant set. This factor, which is not related to the Lyapunov exponents, causes an increase of the slope of $\beta F(\beta)$ for $\beta < \beta_c$. The slope of $\beta F(\beta)$ for $\beta \to -\infty$ is determined by the shortest intervals at each level. Short intervals can be created by pruning. In the complete case without pruning, each level-n interval $I_s^{(n)}$ gives rise to two level-$(n+1)$ intervals $I_{s'}^{(n+1)}$ and $I_{s'+1}^{(n+1)}$, the lengths of both being equal and by a factor η shorter than the length of the "parent" interval $I_s^{(n)}$. When pruning occurs, however, one of the intervals $I_{s'}^{(n+1)}$ and $I_{s'+1}^{(n+1)}$ may be much shorter than the other or even missing. If such very short intervals arise regularly in the $n \to \infty$ limit, this may have the same effect in the free energy as a second Lyapunov exponent greater than $\log \eta^{-1}$. For three special cases, it will be demonstrated that particularly short intervals indeed occur regularly. The sequence of such intervals appears to be particularly simple for $\eta = 1/2$. Similar sequences arise when an arbitrary heteroclinic orbit is pruned. The typical situation is illustrated for the case $\eta = (\sqrt{3} - 1)/2 \simeq 0.366$. Another type of sequence with a second scaling factor arises for more exceptional n values as $\eta = (\sqrt{5} - 1)/2 \simeq 0.618$. For $\eta = 1/2$, both types coincide.

4.1.1. $\eta = 1/2$. In the complete case (i.e., when there is no pruning) the nth image of each interval $I_s^{(n)}$ has length 1. When pruning occurs, the shortest level-n interval $I_{\min}^{(n)}$ has an n-fold iterate $f^{(n)}(I_{\min}^{(n)})$ with lengths significantly less than 1. For $\eta = 1/2$, the $f^{(n)}(I_{\min}^{(n)})$ are displayed in Fig. 6a. Being located at the upper border of the unit square (inside the vertical ellipse), they arise because the branch at $x = 1/2$ of the unstable manifold $(0, 0)$ touches the stable manifold of $(1, 1)$ in P_c. Indeed, there is a sequence of line segments converging to this unstable branch. The lower ends of these line segments (inside the circle of Fig. 6a) fall into the angle

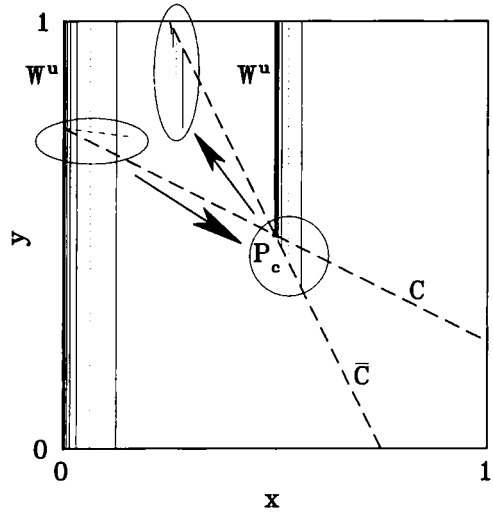
1
W^u
W^u
y
P_c
C
C̄
0
0
1
x

(a)

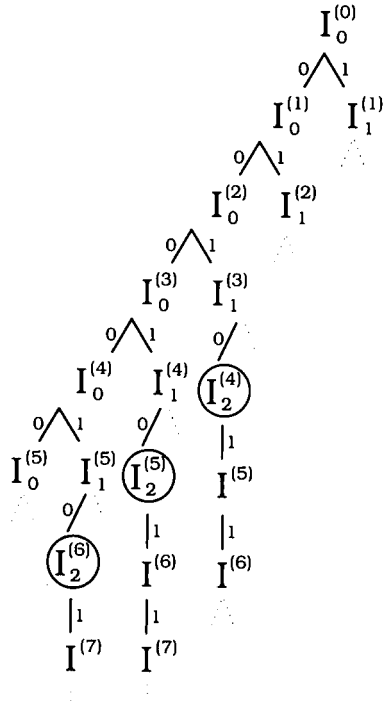
I_0^(0)
I_0^(1)
I_1^(1)
I_0^(2)
I_1^(2)
I_0^(3)
I_1^(3)
I_0^(4)
I_1^(4)
I_2^(4)
I_0^(5)
I_1^(5)
I_2^(5)
I^(5)
I_2^(6)
I^(6)
I^(6)
I^(7)
I^(7)

(b)

formed by the line C and its image $\bar{C}$ in P_c. Being mapped into the vertical ellipse by the lower branch of f in the next step, they will be separated from the remaining (long) parts of the vertical lines, which are mapped by the upper branch of f. Table I shows the symbol sequence and lengths of $I_{\min}^{(n)}$. For $n \geq 4$, the symbol sequences are of the form $(0)^{n-2}10$. Under $n-2$ applications of the lower branch of f, the images $f^{(n-2)}(I_{\min}^{(n)})$ (indicated by the horizontal ellipse in Fig. 6a) are at a distance 2^{2-n} from the left side of the unit square. At the next iteration, $f^{(n-2)}(I_{\min}^{(n)})$ is mapped by the upper branch of f. The $(n-1)$th iterate $f^{(n-1)}(I_{\min}^{(n)})$ is located at a distance 2^{1-n} from the midpoint of the unit square, inside the angle formed by C and $\bar{C}$ (inside the circle in Fig. 6a), and its length is $3/2^n$. After the nth iteration, finally, the iterate $f^{(n)}(I_{\min}^{(n)})$ of the shortest level-n interval has the length $6/2^n$. The interval $I_{\min}^{(n)}$ is shorter by a factor 2^n than its nth image and consequently has the length $l_{\min}^{(n)} = 6/2^{2n}$.

The hierarchical organization of the intervals $I_{\min}^{(n)}$ with scaling factor 2^{-2} is shown in Fig. 4. The lowest interval $I_0^{(2)}$ splits into the intervals $I_0^{(3)}$ and $I_1^{(3)}$. At the next generation, the interval $I_1^{(3)}$ splits into a large upper part labeled $I_3^{(4)}$ and a very small lower part, $I_2^{(4)}$. The latter is the shortest interval on the fourth level and therefore is labeled $I_{\min}^{(4)}$. In the same way, the level-3 interval $I_0^{(3)}$ gives rise to $I_{\min}^{(5)} = I_2^{(5)}$ in the fifth generation, and so on. Thus, a short interval of length $6/2^{2n}$ is created regularly at each level $n \geq 4$.

The scaling factor 2^{-2} of the sequence $\{I_{\min}^{(n)}\}$ is the cause of the slope $2 \log 2$ in the free energy for $\beta \to -\infty$. For sufficiently negative β values the rapid convergence of the series $\{F_1^{(n)}(\beta)\}$ to the asymptotic scattering free energy $F(\beta)$ is due to the constancy of the quotient $l_{\min}^{(n)}/l_{\min}^{(n+1)}$. Figure 6b shows the part of a binary tree containing the $I_{\min}^{(n)}$. The nodes correspond

---

Fig. 6. Second length scaling factor for $\eta = 1/2$. (a) A sequence of short line segments arises because the unstable manifold W^u of (0, 0) (heavy line segments) touches the lines C and $\bar{C}$ (dashed) in P_c. Under $(n-2)$-fold application of f, the lower part of $I^{(0)}$ approaches the left border [unstable manifold of (0, 0)] up to a distance 2^{-n+2}. The parts inside the horizontal ellipse are mapped, by the upper branch of f, inside the angle formed by the lines C and $\bar{C}$ (cf. circle). Being mapped to the upper border of the unit square (cf. vertical ellipse) by the lower branch of f, these short pieces are separated from the longer, upper parts. Their lengths decrease with 2^{-n}, and their preimages on $I^{(0)}$ are the shortest intervals $I_{\min}^{(n)} = I_2^{(n)}$ (cf. Fig. 4). The dotted vertical segments inside the horizontal ellipse, the circle, and the vertical ellipse are the images $f^4(I_{\min}^{(6)})$, $f^5(I_{\min}^{(6)})$, and $f^6(I_{\min}^{(6)})$, respectively. The nearly horizontal dashed line in the horizontal ellipse indicates the upper end of $f^{n-2}(I_{\min}^{(n)})$. (b) The part of a binary tree that contains the intervals $I_{\min}^{(n)} = I_2^{(n)}$. The nodes of the tree correspond to the intervals $I_\lambda^{(n)}$ and the symbols at the links correspond to the symbols in the finite subsequence $\sigma_1 \cdots \sigma_n$ associated with the intervals. The $I_2^{(n)}$ are created regularly at each level. However, the interval $I_2^{(n+1)}$ is not connected to the interval $I_2^{(n)}$ by a simple link (no parent–descendant relation). No branching occurs at the node corresponding to an $I_{\min}^{(n)}$ and at the first $n-3$ nodes below it.

Table I. Symbol Sequences and Lengths of the Shortest Intervals $I^{n}_{\min} \subset I^{(0)}$ for $\eta = 1/2$ and $n = 1, \ldots, 10$[a]

n	Length of $I^{(n)}_{\min}$	Symbol sequence
1	0.25	0
2	0.125	10
3	6.25×10^{-2}	110
4	2.344×10^{-2}	0010
5	5.859×10^{-3}	00010
6	1.465×10^{-3}	000010
7	3.662×10^{-4}	0000010
8	9.155×10^{-5}	00000010
9	2.289×10^{-5}	000000010
10	5.722×10^{-6}	0000000010

[a] For $n \geq 4$, the symbol sequences are of the form $(0)^{n-2}10$ and the lengths are given by $6 \cdot 2^{-2n}$.

to the $I^{(n)}_{s}$ and the symbols at the joints to the next symbols in the sequences associated with the intervals. The nodes corresponding to the $I^{(n)}_{\min}$ are encircled. The structure of the binary tree can be obtained from Fig. 4 by rotating the latter clockwise by 90°. Two points are noteworthy: First, the shortest level-n interval $I^{(n)}_{\min}$ cannot be reached from the interval $I^{(n-1)}_{\min}$ at level $n-1$ by climbing down the tree: There is no parent–descendant relation between $I^{(n-1)}_{\min}$ and $I^{(n)}_{\min}$: It is not $I^{(n-1)}_{\min}$ that gives rise to $I^{(n)}_{\min}$. Second, the branch starting out of the node corresponding to $I^{(n)}_{\min}$ continues for $n-2$ steps without embranchments. This means that the interval $I^{(n)}_{\min}$ will not be divided further until level $2n-2$. The length of $I^{(n)}_{\min}$ does not change before that level. Thus, the time delay for all trajectories starting out of the interval $I^{(n)}_{\min}$ is greater than or equal to the value $2n-2$.

Sequences $\{I^{(n)}_{s_n}\}$ of intervals with scaling η^2 do start at each level of the binary tree. Their number and length are estimated in the Appendix, yielding the partition sum [Eq. (A3)]

$$Z^{N}(\beta) \propto \exp[K_0 N(1+\beta/\beta_c)] \times \{C_1(\beta, K_0) + C_2(\beta, K_0)\exp[K_0 N(-1+\beta/\beta_c)]\} \tag{4.1}$$

with $\beta_c = -K_0/\ln 2$. The constants C_1 and C_2 are independent of N. Being determined only by the leading term in Eq. (4.1), the asymptotic free energy reads [cf. Eq. (A7)]

$$\beta F(\beta) \equiv \lim_{n \to \infty} \beta F^{(n)}(\beta) = \begin{cases} -K_0 + \beta \log 2 & \text{if } \beta \geq -K_0/\log 2 \\ 2\beta \log 2 & \text{otherwise} \end{cases} \tag{4.2}$$

Thus, for $\eta = 1/2$, the scattering free energy displays a phase transition at $\beta_c = -K_0/\log 2 < 0$, as indicated by the dotted line in Fig. 5.

4.1.2. $\eta = (\sqrt{3}-1)/2$. For $\eta = 1/2$, the sequence of line segments with a second scaling factor arises because the unstable manifold of a fixed point touches the stable manifold of a fixed point in P_c, where the line C and its image $\bar{C}$ intersect. This very particular constellation does not occur for typical parameter values.

For $\eta < 1/2$, the chaotic saddle of f is embedded in a 2D Cantor set with scaling η (Fig. 3b). The level-k approximation of the Cantor set is composed of 4^k squares of linear size η^k (called k-squares). Since the upper sides of the k-squares belong to the stable manifold of (1, 1) and the left sides to the unstable manifold of (0, 0), all upper left corners correspond to heteroclinic intersections. As in the previous subsections, a sequence of line segments with a second length scaling arises if a branch of the unstable manifold touches the stable manifold without intersecting it. Such a situation occurs when the line $\bar{C}$ intersects the not yet pruned upper left corner of a k-square.

For $\eta = (\sqrt{3}-1)/2 \simeq 0.366$, for example, the line $\bar{C}$ intersects the 2-square A in Fig. 7a. As in Fig. 6a, the nth iterates of the lowest-lying level-n intervals $I_0^{(n)} \subset I^{(0)}$ approach the left side of the unit square up to a distance η^{n+1} (Fig. 7a). The images of their upper parts above the line C extend from the line $\bar{C}$ up to the $(y = 1)$-line. Their lower ends (near the point P_{ul}) form a sequence of line segments of length η^n running into the angle formed by the line $\bar{C}$ and the upper side of A (instead of the line C as in the previous subsection). After two further steps of iteration, when the upper side of A is mapped onto the upper side of the unit square, these short segments are separated from the rest. Their preimages on the line $I^{(0)}$ with symbol sequences $(0)^n\,100$ form a sequence of intervals with scaling η^2 (Table II).

The part of the binary tree containing the $I_{\min}^{(n)}$ (Fig. 7b) is very similar to that for the $\eta = 1/2$ case. The $I_{\min}^{(n)}$ also occur regularly at each step, but one level later than the corresponding intervals in Fig. 6b. As for the case $\eta = 1/2$, the number of sequences with a second scaling factor can be estimated using the reasoning in the Appendix. The scattering free energy reads, in analogy with Eq. (4.2),

$$\beta F(\beta) \propto \begin{cases} -K_0 + \log \eta^{-1} & \text{if} \quad \beta \geqslant -K_0/\log \eta^{-1} \\ 2\beta \log \eta^{-1} & \text{otherwise} \end{cases} \tag{4.3}$$

The convergence is uniform as in the $\eta = 1/2$ case. Therefore, the functions $F_1^{(n)}$, which are shown in Fig. 7c, yield the best numerical results.

4.1.3. $\eta = (\sqrt{5}-1)/2$. For $\eta \geq 1/2$, it is possible that P_c is touched by the unstable manifold of a *periodic* orbit. We show that also in such a case an argument analogous to that for the $\eta = 1/2$ case is possible and prove the existence of an additional scaling factor. For $\eta = (\sqrt{5}-1)/2 \simeq 0.618$, the period-6 orbit $\overline{000111}$ fulfills the above condition (cf. Fig. 8a). The coordinates of the points of this orbit are displayed in Table III. Two points lie on the $x = 1/2$-line, one (P) above $y = 1/2$, the other below. Figure 8a displays the first images of the upper end of the interval

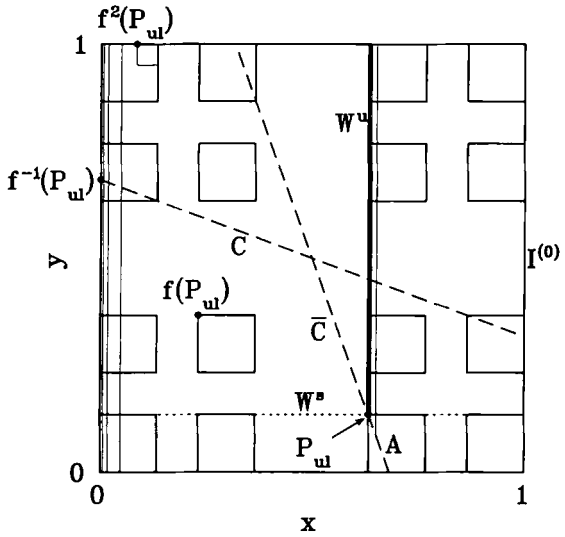

(a)

Fig. 7. Second length scaling factor for $\eta = (\sqrt{3}-1)/2$. (a) The scenario giving rise to short line segments is similar to that exposed in Fig. 6a. The unstable manifold W^u touches the upper left corner P_{ul} of the 2-square A. Parts of the n-fold iterates of $I^{(0)}$ approach the left border of the unit square at the rate η^n. The parts of these images near $f^{-1}(P_{ul})$ are mapped inside the angle formed, at P_{ul}, by the line $\bar{C}$ (dashed) and the upper side of A, which belongs to the stable manifold W^s of (1, 1) (dotted line). Being mapped under twofold iteration of f, to the upper border of the unit square near $f^2(P_{ul})$, the pieces inside the angle are separated from the long parts of the line segments. The lengths of the short pieces scale with η, giving rise to the scaling factor η^2 in the sequence of preimages $I^{(n)}_{\min} \subset I^{(0)}$. (b) Part of a binary tree displaying the nodes corresponding to the $I^{(n)}_{\min}$. The tree is similar to the one in Fig. 6b. The main difference is that in the present figure, the corresponding intervals of minimal length occur one step later. This is due to the fact that W_u touches the line $\bar{C}$ at the corner of a 2-square [cf. part (a)] while in Fig. 6a, the contact occurs in P_c, which is the corner of a 1-square. (c) Free energy $\beta F_1^{(n)}(\beta)$ calculated by the scattering method for $\eta = (\sqrt{3}-1)/2$ and $n = 12$, 15, 18, 20, and 22. For all β values, the series of functions converges well to the asymptotic function (solid line). The dotted line indicates the value of β_c.

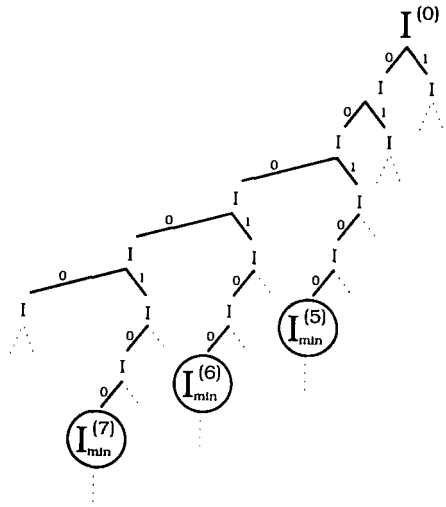

(b)

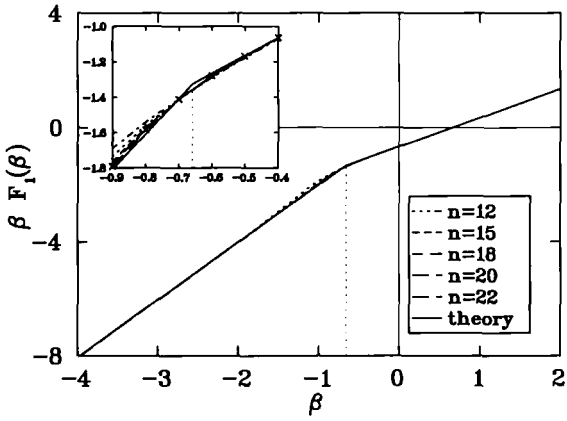

(c)

Fig. 7. (*Continued*)

Table II. Symbol Sequences and Length of $I^n_{\min}$ for $\eta = (\sqrt{3}-1)/2 \simeq 0.366$ and $n = 1, \ldots, 10^a$

n	Length of $I^{(n)}_{\min}$	Symbol sequence
1	3.170×10^{-1}	0
2	8.494×10^{-2}	01
3	3.109×10^{-2}	101
4	1.138×10^{-2}	1101
5	4.165×10^{-3}	11101
6	8.802×10^{-4}	000100
7	1.179×10^{-4}	0000100
8	1.580×10^{-5}	00000100
9	2.117×10^{-6}	000000100
10	2.836×10^{-7}	0000000100

[a] For $n \geqslant 6$, the symbol sequences are of the form $0^{n-3}100$ and the lengths are given by η^{2n-5}.

$I_0^{(1)} \subset I^{(0)}$. These images approach the periodic orbit in spirals: after $6k+4$ steps of iteration ($k \geqslant 0$), it starts at the height of the point P, and its horizontal distance from this point is $((1-\eta)/2)\,\eta^{6k+4}$. Consequently, $f^{(6k+4)}(I_0^{(1)})$ contains a short line segment inside the angle formed by C and $\bar{C}$, analogously to the short line segments shown in Fig. 6a. The sequence of these line segments scales with η. The only difference is that now they arise only at every sixth step (Table IV). Being shorter than the $(6k+4)$th image by a factor η^{6k+4}, the preimages of these line segments give rise to a sequence of $I^{(6k+4)}_{\min}$ that scales with η^2. A reasoning analogous to the one given in the Appendix leads again to Eq. (4.3).

We have argued that very short intervals $I^{(n)}_{\min}$ are only created on any sixth level of the corresponding binary subtree. This has no influence on the limiting form of $\beta F(\beta)$, but it is reflected in the convergence properties of the $\{F^{(n)}\}$ and the $\{F^{(n)}_k\}$: the best convergence is obtained by the finite-level approximation of the form $\{F^{(n)}_6\}$, which has been used for calculating the numerical results shown in Fig. 8b.

4.2. Generalization

In this section, we argue that the second length scaling factor and the anomalous phase transition at $\beta_c = -K_0/\log \eta^{-1}$ are present for η values belonging to a dense subset of the parameter interval. The starting point of the following reasoning is the observation that new interdictions arise at the special parameter values of the examples: the orbit described by the symbol sequence $(0)^\infty\, 10(1)^\infty$ is pruned at $\eta = 1/2$; the orbit $(0)^\infty\, 100(1)^\infty$

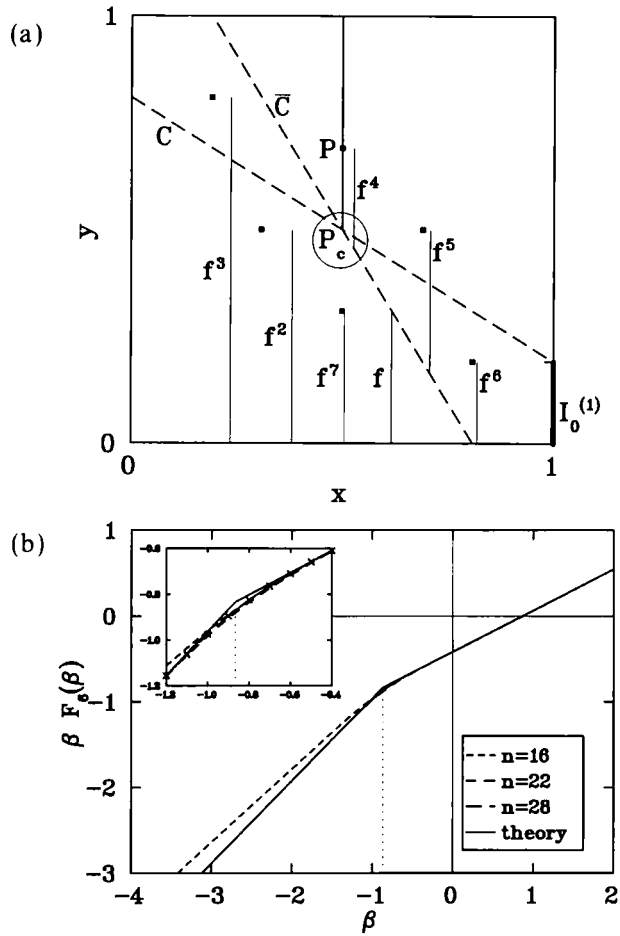

Fig. 8. Second length scaling factor for $\eta = (\sqrt{5}-1)/2$. (a) The black boxes indicate the points of the period-6 orbit with symbol sequence $\overline{000111}$. The vertical line at $x = 1/2$ is a part of the unstable manifold of this orbit. It touches the lines C and $\bar{C}$ (dashed) in P_c. Under n-fold iteration, the interval $I_0^{(1)} \subset I^{(0)}$ (heavy lower part of the right border of the unit square extending up to the intersection of C with $I^{(0)}$) approaches the unstable manifold of the orbit in spirals (light vertical lines labeled f^n). After $n = 6k + 4$ iterations, a part of $f^n(I_0^{(1)})$ is located at the distance $(1-\eta)\eta^n/2$ from the point P. The lower end of this line segment touches $\bar{C}$ near P_c (cf. circle). As in the $\eta = 1/2$ case (cf. Fig. 6a), the piece inside the angle formed by C and $\bar{C}$ is separated from the long upper part of the line segment in the next step. Thus, a short piece with length $\propto \eta^n$ arises at each step $n = 6k + 5$. The nth preimages form a sequence of intervals $I_{\min}^{(n)}$ with scaling η^2. (b) Free energy $\beta F_6^{(n)}(\beta)$ calculated by the scattering method for $\eta = (\sqrt{5}-1)/2$ and $n = 16$, 22, and 28. Owing to the periodicity in the occurrence of the $I_{\min}^{(n)}$, the function βF_6 converges rapidly for all values of β. The dotted line indicates the value of β_c.

Table III. Iterates of the Period-6 Orbit with Symbol Sequence 000111 for $\eta = (\sqrt{5}-1)/2 \simeq 0.618$[a]

$(1/2, \eta/2)$	
$((1+\eta)/2, (1-\eta)/2)$	
$((2-\eta)/2, 1/2)$	P
$(1/2, (2-\eta)/2)$	
$((1-\eta)/2, (1+\eta)/2)$	
$(\eta/2, 1/2)$	

[a] The label P refers to the point indicated in Fig. 8a.

Table IV. Symbol Sequences and Lengths of the Shortest Intervals for $\eta = (\sqrt{5}-1)/2 \simeq 0.618$ and $n = 1, \ldots, 17$[a]

n	Length of $I_{\min}^{(n)}$	Symbol sequence
1	1.910×10^{-1}	0
2	1.180×10^{-1}	10
3	7.295×10^{-2}	110
4	3.444×10^{-2}	0001
5	4.065×10^{-3}	00010
6	2.512×10^{-3}	000101
7	1.553×10^{-3}	0001011
8	9.597×10^{-4}	00010111
9	8.654×10^{-5}	000000110
10	5.348×10^{-5}	1000000110
11	1.263×10^{-5}	00011100010
12	7.803×10^{-6}	000111000101
13	4.822×10^{-6}	0001110001011
14	2.980×10^{-6}	00011100010111
15	2.687×10^{-7}	000000111100100
16	1.661×10^{-7}	1000000111100100
17	3.921×10^{-8}	00011100011100010

[a] For $n = 6k-1$, the symbol sequences are of the form $000(111000)^{k-1}10$ and their lengths are given by $(1-\eta^2)(1-\eta)\,\eta^{2n-3}/2$.

is pruned at $\eta = (\sqrt{3}-1)/2$; and the orbit $(000111)^{\infty}\,0000(111000)^{\infty}$ is pruned at $\eta = (\sqrt{5}-1)/2$. This coincidence is not fortuitous: the conditions giving rise to a sequence of line segments with a second scaling factor arise exactly at parameter values at which bifurcations cause the interdictions of orbits of the invariant set.

Pruning in a smooth horseshoe occurs via inverse saddle node bifurcations, which are related to homoclinic or heteroclinic tangencies. In the invariant set of the piecewise linear maps f, the bifurcations associated with pruning can be considered as degenerate saddle node bifurcation. Indeed, Eq. (2.1) is a limiting case of a family of smooth maps studied in ref. 12, which display a chaotic invariant set obtained by an S-shaped double-horseshoe construction. The map f is obtained if the width of the middle leg of the double horseshoe shrinks to zero and degenerates to the critical line. The corresponding parts of the invariant set disappear in this limit, and the remaining branches of the invariant manifolds degenerate to disconnected straight line segments. Accordingly, homoclinic and heteroclinic tangencies transform into "contacts," which means that a branch of a stable and a branch of an unstable manifold touch without tangency and intersection. Bifurcations due to such contacts also occur in the scattering system studied in ref. 16.

Figure 9 displays the type of bifurcation that occurs at $\eta_0 = (\sqrt{3}-1)/2$, when the end of a segment of the unstable manifold (cf. arrow) touches a branch of the stable manifold. It is precisely this point of contact that is

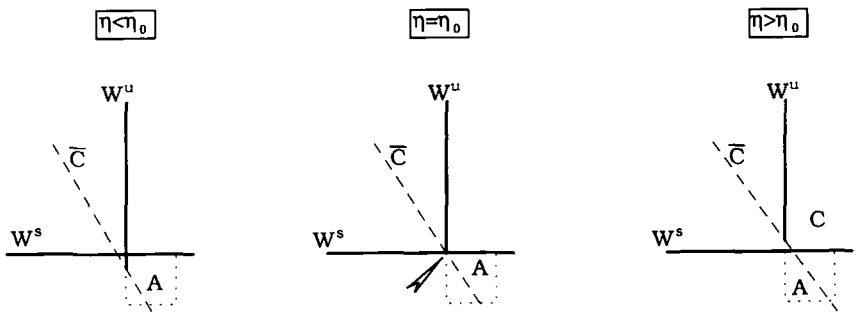

Fig. 9. Bifurcation scheme for the bifurcation arising at $\eta_0 = (\sqrt{3}-1)/2$. The three parts of the figure illustrate the situation for $\eta < \eta_0$, $\eta = \eta_0$, and $\eta > \eta_0$. The line segments labeled by W_s and W_u, respectively, belong to the stable manifold of (1, 1) and to the unstable manifold of (0, 0). The vertical line segment ends at the line $\bar{C}$. The manifold W_s contains the upper side of the 2-square A, and W_u contains, for $\eta < \eta_0$, the not yet pruned part of the left side of A. For $\eta < \eta_0$, W_s and W_u intersect; for $\eta > \eta_0$, the intersection is lost. At $\eta = \eta_0$, when W_u touches W_s at the corner P_{ul} of A (arrow), the orbit passing through P_{ul} becomes forbidden. This is the situation in which a series of line segments with a second scaling factor arises (cf. Fig. 7a).

responsible for the second scaling factor because it gives rise to a sequence of short line segments running into the angle formed, at P_{ul}, by $\bar{C}$ and the stable manifold W^s (Fig. 7a). Since the branch of W^s which contains the upper border of the k-square A is mapped onto the upper border of the unit square after at most k iterations, the short pieces inside the angle are necessarily separated from the remaining longer parts after this number of iterations.

The heteroclinic contact can occur at the upper left corner of any not yet pruned k-square. It signifies pruning of a heteroclinic orbit of the form $(0)^\infty \sigma_{-k+1} \cdots \sigma_k (1)^\infty$ at the corresponding η value. The middle subsequence of length $2k$ labels the k-square where the heteroclinic contact occurs.

For $\eta > 1/2$, there is no longer an embedding Cantor set (Fig. 3d). However, new interdictions of heteroclinic orbits of the form $(1)^\infty \sigma_{-k+1} \cdots \sigma_k (0)^\infty$ still arise at those η values, and the subsequence $\sigma_{-k+1} \cdots \sigma_k$ still describes a k-square.[13] Thus, the scenario displayed in Fig. 9 also occurs for $\eta > 1/2$. Hence, we expect the second length scaling factor η^2 and the anomalous phase transition at $K_0/\log \eta$ to be present for all η values at which heteroclinic orbits of the invariant set become forbidden. If, however, k is larger than about 20 or 30, the convergence can no longer be observed numerically. This is why the numerical calculations of $F_1^{(n)}(\beta)$ and $F^{(n)}(\beta)$ did not allow any statement about the asymptotic free energy for η values *slightly* different from 1/2, where the newly pruned heteroclinic orbit, if there is any, presumably exhibits large values of k.

Numerical results for the parameter dependence of the topological entropy obtained by investigating periodic orbits[15] strongly indicate that $K_0(\eta)$ is strictly monotonically decreasing. Hence, new interdictions occur at least in a dense subset of the parameter interval $[1/3, 1]$. Since heteroclinic orbits as well as periodic orbits lie dense in the chaotic invariant set, new interdictions of heteroclinic orbits are expected to occur also in a dense subset of the parameter interval. For the parameter values of this subset, the free energy has the slope $2 \log \eta^{-1}$ for $\beta < \beta_c < 0$, and an anomalous phase transition occurs at $\beta_c = K_0/\log \eta$.

Finally, notice that the situation treated in Section 4.1.3 corresponds to a somewhat different type of bifurcation. For $\eta = (\sqrt{5} - 1)/2$, the contact occurs between the end of an unstable branch and the end of a stable branch. Both manifolds belong to the period-6 orbit. In such a case, we expect an anomalous scaling only if the contact takes place in the center P_c of the unit square. The reason is that the stable manifold of a periodic orbit is not mapped onto the border of the unit square. Therefore, the intersection of C and $\bar{C}$ is needed to separate the short pieces from the longer parts, and these lines always intersect in P_c. The bifurcation caused by the

contact of two *ends* of straight line segments at P_c is not generic. Indeed, even for $1/2 < \eta < 1$, there are whole subintervals for which P_c is not a point of the chaotic saddle and therfore an anomalous behavior of the scattering free energy caused by *this* kind of bifurcation is not expected.

5. DISCUSSION AND SUMMARY

The thermodynamics of the geometric properties of a chaotic saddle has been investigated for a class of piecewise linear, area-preserving maps. By a numerical scattering experiment, we calculated the time delay function for orbits starting out of a line $I^{(0)}$ crossing the stable manifolds of the saddle. The partition sum has been obtained by means of the lengths of level-n intervals, for which the delay time takes at least the value n. For appropriate values of η, the scattering free energy obtained in this way displays a second scaling exponent for $\beta < \beta_c < 0$ and a phase transition at $\beta_c = K_0/\log \eta$. This happens in spite of the fact that the Lyapunov exponents of these maps are constant everywhere.

The fact that an additional scaling exponent and a phase transition are present in the scattering free energy even though they do not occur in the free energy obtained by summing over the periodic orbits indicates that these two quantities need not to be identical. Indeed, the theoretical analysis in Section 4 shows that both features are solely due to pruning. They occur when a branch of an unstable manifold touches a branch of a stable manifold without intersecting it. This contact between invariant manifolds (which is not a tangency for these maps) has the effect that on the line of initial conditions, a sequence of particularly small intervals $I_{\min}^{(n)}$ arises in the course of iteration. While in general the lengths of the level-n intervals scale with η, the lengths of the $I_{\min}^{(n)}$ scale with η^2. This gives rise to the second scaling exponent in the free energy. The phase transition occurs because the number of intervals with the anomalous scaling factor increases slower than $e^{K_0 n}$.

Obviously, there is no difference between the scattering free energy and the spectrum of Lyapunov exponents when the critical line passes through the gaps of the embedding Cantor set without touching any point of the invariant set. In such a case, which may arise when the critical line is displaced while η is fixed to some value less than 1/3, the map is still hyperbolic in whole subintervals of the parameter interval, even in the presence of pruning. In these subintervals, no new interdictions arise; this results in plateaus in the topological entropy as a function of the displacement of the critical line.[17] In the present setting, however, the critical line is fixed symmetrically with respect to the invariant set and the eigenvalue η of the map is taken as control parameter. There is strong numerical

evidence that in this case, new interdictions of orbits occur on a dense subset of the parameter interval $[1/3, 1]$.[15]

Interdictions are caused by inverse bifurcations. This means that somewhere in the invariant set, homoclinic and heteroclinic manifolds touch without intersecting. Bifurcations in the invariant set imply the breakdown of hyperbolicity. This also holds for maps of the form (2.1), even though there is no effect on the Lyapunov exponents. Thus, the anomalous length scaling factor and the anomalous phase transition in the scattering free energy indicate that at the corresponding parameter values bifurcations and consequently new interdictions of orbits occur in the chaotic invariant set.

The occurrence of a phase transition at negative β values is similar to what happens for the logistic map.[18] In that case, however, the second scaling factor is not due to pruning, but to the slope of the logistic map at $x=0$; the shortest interval at level n is contained in the shortest interval at level $n-1$; in the binary tree, both intervals are directly related by a link. In the present case, the intervals $I_{\min}^{(n)}$, which are organized on a binary tree as shown in Fig. 6b, are not related by a parent–descendant relation. The series $\{I_{\min}^{(n)}\}$ converges, in the limit $n \to \infty$, to a point outside all the $I_{\min}^{(n)}$. This is why this series can exhibit a length scaling exponent not related to the Lyapunov exponents of the dynamical system.

For maps with the same kind of singularity as the one present in Eq. (2.1) (Lorenz-type maps[14]), an anomalous phase transition is also expected to exist. The essential ingredient seems to be the fact that the bifurcation is degenerate with a missing stable branch. The degeneracy of the inverse saddle node bifurcation is closely related to the existence of a line of singularities in the map. As a consequence, the invariant manifolds are degenerated to disconnected line segments. In such a situation no KAM tori are associated with pruning. KAM tori would perhaps prevent the occurrence of the anomalous scaling and the phase transition. However, even when a line of singularities exists, the anomalous scaling exponent may, in a repellor with multifractal properties, be masked by the spectrum of Lyapunov exponents if the anomalous scaling exponent is less than the maximal Lyapunov exponent.

APPENDIX. EVALUATION OF THE PARTITION SUM

In order to evaluate the partition sum, we estimate the number and the length of intervals with the anomalous length scaling η^2. The reasoning is displayed for the $\eta = 1/2$ case. For the other cases, it goes along the same line and yields the same results.

There is a series $\{I_{\min}^{(n)}\}$ of shortest intervals with length $6/2^n$, which is

displayed in Fig. 4. The intervals $I_{\min}^{(n)}$ remain unchanged (survive) from level n to level $2n-2$. This is indicated in the binary tree shown in Fig. 6b: The nodes corresponding to $I_{\min}^{(n)}$ and its descendants up to level $2n-3$ have no branching. To the series $\{I_{\min}^{(n)}\}$ we associate a subtree which consists of the part shown in Fig. 6b together with the parts without branching related to the $I_{\min}^{(n)}$. Notice that such a subtree can spring off at each level k of the whole binary tree. The length of a short interval that is created at the nth level of a kth-order subtree [i.e., at the $(n+k-1)$th level of the main tree] has the length $6/2^{2n+k-1}$. This interval remains unchanged from level $n+k-1$ to level $2n+k-3$.

To give an upper limit for the number of intervals with scaling 2^{-2}, we assume that every level-k node with branching that does not belong to a lower-order subtree gives rise to a new kth-order subtree. On the average, the number of level-k nodes with branching is governed by the topological entropy and evaluates to $(e^{K_0}-1)\,e^{K_0(k-1)}$. From this number, we must subtract one node for each subtree arising at level $k' < k$. (The other level-k nodes of the subtree have no branching or may serve as origin for a new subtree.) The subtraction has an influence only on the constant prefactor. The number of new subtrees arising at level k is still proportional to e^{kK_0}.

Counting the intervals, one must distinguish two cases. For order-n intervals with $4 \leqslant n \leqslant N/2$, the intervals arising in low-order subtrees do not survive up to level N. Thus, only kth-order subtrees satisfying the relation $N-2n+3 \leqslant k \leqslant N-n+1$ have to be taken into account. Summing over the values of n and the allowed values of k, we get the contribution

$$A \propto 6^{\beta} \sum_{n=4}^{N/2} \sum_{k=N-2n+3}^{N-n+1} 2^{-(2n+k)\beta} \cdot e^{K_0(k-1)} \tag{A1}$$

For $(N+2)/2 \leqslant n \leqslant N$, all values of k between 1,..., $N-n+1$ are allowed. Thus, the second contribution reads

$$B \propto 6^{\beta} \sum_{n=N/2+1}^{N} \sum_{k=1}^{N-n+1} 2^{-(2n+k)\beta} \cdot e^{K_0(k-1)} \tag{A2}$$

The level-N partition sum $Z^{(N)}(\beta)$ is the sum of both terms. Summing up the geometrical series in Eqs. (A1) and (A2) and regrouping the terms yields

$$\begin{aligned} Z^N(\beta) &\propto \exp[K_0 N(1+\beta/\beta_c)] \\ &\times \{C_1(\beta, K_0) + C_2(\beta, K_0) \exp[K_0 N(-1+\beta/\beta_c)]\} \end{aligned} \tag{A3}$$

with a prefactor independent of β and N. The "temperature" takes the

value $\beta_c = -K_0/\log 2 < 0$, and the factors $C_1(\beta, K_0)$ and $C_2(\beta, K_0)$ are given by

$$C_1(\beta, K_0) = \frac{(3/2)^\beta e^{-3K_0}}{e^{K_0}(e^{-K_0(1+\beta/\beta_c)} - 1)} \times \left(\frac{2^{-\beta} e^{-3K_0}}{1 - e^{-2K_0}} - \frac{2^{-3\beta}}{1 - e^{-K_0(1-\beta/\beta_c)}} \right) \tag{A4}$$

(A5)

$$C_2(\beta, K_0) = \frac{(3/2)^\beta}{e^{K_0}(e^{-K_0(1+\beta/\beta_c)} - 1)} \times \left(\frac{1}{1 - e^{-K_0(1-\beta/\beta_c)}} - \frac{1}{1 - 4^{-\beta}} \right) \tag{A6}$$

Note that at constant N, the factors C_1 and C_2 diverge like $|\beta - \beta_c|^{-1}$ for $\beta \to \beta_c$. Thus, the limits $N \to \infty$ and $\beta \to \beta_c$ do not interchange. In the limit $N \to \infty$, which has to be taken at constant β, we obtain

$$Z(\beta) = \begin{cases} C_1(\beta, K_0) \exp[K_0 N(1 + \beta/\beta_c)] & \text{if } \beta > \beta_c \\ \frac{1}{2}(\frac{3}{2})^{\beta_c} \sinh^{-1}(K_0) \cdot N \exp(2K_0 N) & \text{if } \beta = \beta_c \\ C_2(\beta, K_0) \exp[2K_0 N \beta/\beta_c] & \text{if } \beta < \beta_c \end{cases} \tag{A7}$$

Taking into account only the leading term for the free energy, one immediately gets Eq. (4.2).

ACKNOWLEDGMENTS

The authors are greatly indebted to Z. Kovács and T. Tél for long and extensive discussions. The financial support of the Swiss National Science Foundation is gratefully acknowledged.

REFERENCES

1. M. J. Feigenbaum, M. H. Jensen, and I. Procaccia, *Phys. Rev. Lett.* **56**:1503 (1986); T. Bohr and D. Rand, *Physica* **25D**:387 (1987); T. Bohr and T. Tél, in *Directions in Chaos*, Vol. II, Hao Bai-lin, ed. (World Scientific, Singapore, 1988); R. Badii, *Rivista del Nuovo Cimento* **12**(3):1 (1989); R. Artuso, E. Aurell, and P. Cvitanovic, *Nonlinearity* **3**:325, 361 (1990).
2. P. Grassberger and I. Procaccia, *Physica* **13D**:34 (1984).
3. Z. Kovács and T. Tél, *Phys. Rev. Lett.* **64**:1617 (1990); Y. T. Lau, J. M. Finn, and E. Ott, *Phys. Rev. Lett.* **66**:978 (1991); Q. Cheng, M. Z. Ding, and E. Ott, *Phys. Lett.* **156**:48 (1991); T. Tel, *Phys. Rev. A* **44**:1034 (1991).

4. T. Tel, *Z. Naturforsch.* **43a**:1154 (1988) and references therein.
5. A. J. Lichtenberg and M. A. Lieberman, *Regular and Stochastic Motion* (Springer-Verlag, Berlin, 1983).
6. R. Lozi, *J. Phys.* (Paris) **39**(C5):9 (1978).
7. T. Tél, *Phys. Lett.* **97A**:219 (1983).
8. P. Reichert and R. Schilling, *Phys. Rev. B* **32**:5731 (1985).
9. R. Schilling, in *Nonlinear Dynamics in Solids*, H. Thomas, ed. (Springer, Berlin, 1992).
10. J. Vollmer, The Topological Entropy of an Inclined Billiard in a Gravitational Field, *Z. Naturforsch.*, to appear.
11. M. Hénon, *Physica D* **33**:132 (1988).
12. W. Breymann and C. Jung, *Europhys. Lett.* **25**(7):509 (1994).
13. J. Vollmer and W. Breymann, Symbolic Dynamics for a Pruned Baker Map, submitted to *J. Phys. A: Math. Gen.*
14. P. Szépfalusy and T. Tél, *Physica* **16D**:252 (1985).
15. J. Vollmer, W. Breymann, and R. Schilling, *Rev. Phys. B* **47**:11767 (1993); J. Vollmer and W. Breymann, *Helv. Phys. Acta* **66**:91 (1993).
16. G. Troll, *Physica D* **50**:276 (1991).
17. P. Häner and R. Schilling, *Europhys. Lett.* **8**:129 (1989).
18. D. Katzen and I. Procaccia, *Phys. Rev. Lett.* **58**:1169 (1987).